

Reducing distance dependent bias in low-cost single frequency GPS network to complement dual frequency GPS stations in order to derive detailed surface deformation field

H.-Y. Chen^{*1}, L.-C. Kuo¹, J.-C. Lee¹, H. Tung¹, S.-H. Su¹, S.-S. Yao² and H. Lee³

A total of 17 low-cost single-frequency L1 global positioning system (GPS) receivers with real-time internet transmission have been set up to intensify the pre-existing network of continuously operating reference stations (CORS) in southeastern Taiwan since 2008. The main objective of this study is to investigate the validity and uncertainty of the L1 stations in southeastern Taiwan. It is well known that the main error source of single-frequency GPS relative positioning in low latitude areas comes from an atmospheric delay, even if the relative distance is only a few kilometres. In this study, two methods of correction algorithms, including adopting local ionospheric models and applying correction terms from local CORS, are tested to estimate the long-period accuracy of station positioning. Our results indicate that the standard deviation of calibrated relative positioning is in a linear trend with respect to the baseline length. The derived positioning accuracies from applying correction terms from CORS provide satisfactory results with the linear ratios of standard deviation/baseline of 0.11 ± 0.02 , 0.12 ± 0.02 , 0.44 ± 0.06 mm km⁻¹ in the north, east and up component, respectively for relative distances under 30 km. The corresponding positioning scatterings amount to 3, 3 and 13 mm, in the north, east and up component, respectively. Although the use of a local ionospheric model algorithm can significantly reduce positioning variation, especially in the north component, the use of the correction terms method yields the best positioning results for three components, horizontal and vertical.

Keywords: Low-cost, CORS, Active fault, Ionospheric model

Introduction

The surface deformation in the southernmost Longitudinal Valley (LV) of eastern Taiwan is mainly accommodated by a complex system of faulting (Fig. 1), which comprises three major active faults, namely the Lichi fault, the Luyeh fault (Yu *et al.*, 1990; Lee *et al.*, 1998; Yu and Kuo, 2001), and the likely blind Central Range fault (Biq, 1965; Lu and Hsu, 1992; Wu *et al.*, 2006; Shyu *et al.*, 2008; Chen *et al.*, 2012). Tectonically, it is located at the suture zone between the Luzon arc of the Philippine Sea plate (i.e. the Coastal Range in Fig. 1) and the Chinese continental margin of the Eurasian plate (i.e. the Central Range). The convergence rate is

about 8.2 cm/year, while one-third of horizontal shortening of about 3 cm/year is being absorbed across the southern LV (Yu *et al.*, 1990; Yu and Kuo, 2001).

Recent global positioning system (GPS) and precise levelling results from mostly campaign-mode surveys combined with 10 continuously operating reference stations (CORS) indicated that the velocity fields of horizontal and vertical components vary in different faults and in different locations in this area (Chen *et al.*, 2012; Chen *et al.*, 2013) (Fig. 1). It is thus necessary to examine the time-series data of higher temporal solution, such as continuous GPS data, in order to characterise the fault slip behaviour in more detail. On the one hand, 10 dual-frequency CORS have been gradually installed since 1994 and are maintained by different agencies in this area. On the other hand, 17 single-frequency receivers (L1 stations) have also been installed several years ago, in order to densify the 10-station GPS CORS network with three main goals in mind:

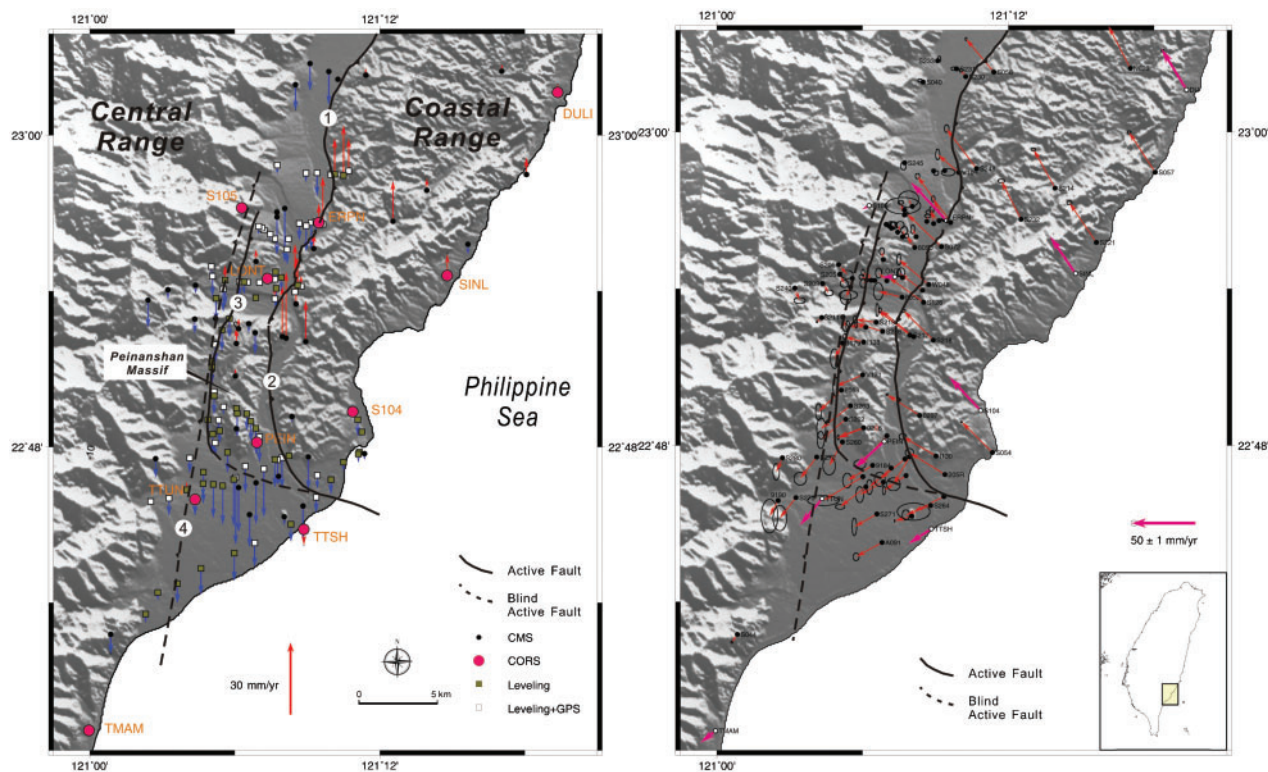
- (i) to better determine the near-fault deformation in detail

¹Institute of Earth Sciences, Academia Sinica, PO Box 1-55 Nankang, Taipei 11529, Taiwan

²Department of Real Estate Development and Management, Kun Shan University, No. 949 Da-Wan Rd., Tainan 71003, Taiwan

³Department of Civil Engineering, Changwon National University, 9 Sarim-dong, Changwon, Gyeongnam 641-773, Korea

*Corresponding author, email chenhy@earth.sinica.edu.tw



1 Velocity field of the near-fault GPS array in the Taitung area. The left graph shows the vertical velocities (Chen *et al.*, 2012) and the right graph presents the horizontal velocities relative to the ITRF2005 reference frame (Chen *et al.*, 2013). Black lines represent major active faults: Chihshang Fault (1), Lichi Fault (2), Luyeh Fault (3), Central Range Fault (4)

- (ii) to better characterise the slip behaviour of the three major active faults and other possible active faults
- (iii) to obtain highly precise positioning using low-cost equipment.

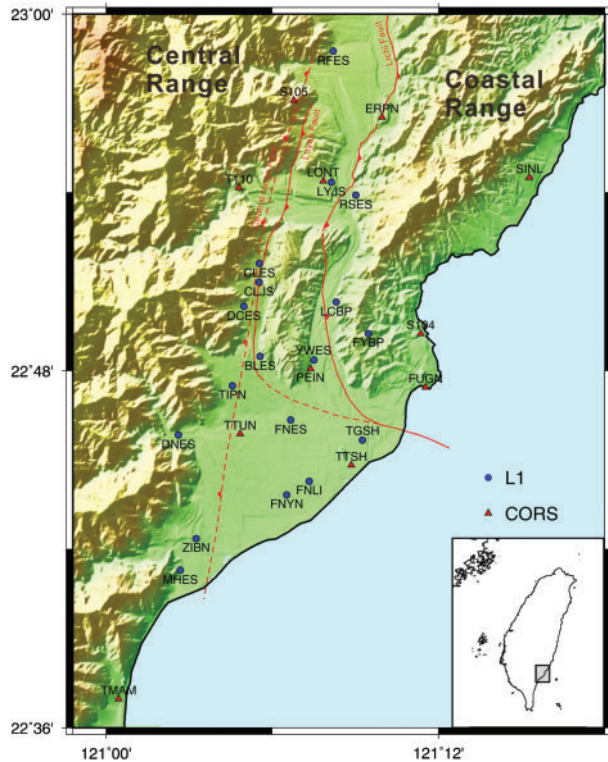
This paper is focused on the third point, that is, to investigate whether the single frequency L1 stations can provide reliable, precise positioning and to what extent in this particular study area.

For the purposes of geodetic monitoring and surface deformation detection using GPS measurements, dual-frequency receivers are the most common and reliable instrument thanks to the fact that the ionospheric delay can be mitigated by linear combination of two frequency signals and the positioning accuracy has been proven to be at the centimetre level, even over long baselines up to 2000 km (Blewitt, 1989). To study the near-fault deformation, another practical strategy is to conduct campaign-mode surveys on an annual or seasonal basis utilising geodetic (dual-frequency) receiver, thereby avoiding the relatively high cost of installing and maintaining CORS. In the case of a campaign survey, several receivers, skilled operators and transportation need to be organised to re-occupy stations and acquire periodic data (results shown in Fig. 1). Considering the research expense limitation and the accuracy requirements, another plausible method would be a network of low-cost single-frequency (L1) receivers. As shown by the previous estimation, the accuracy of station positioning is comparable to the result from dual-frequency receivers (Rizos *et al.*, 2000). Meanwhile, the L1 receiver network has the advantage of providing a continuous data stream to record detailed movement for the near-fault study. However, for a L1 GPS receiver, the

ionospheric delay bias cannot be mitigated by using the ionosphere-free linear combination (of L1 and L2 dual-frequency observations). An algorithm utilising a long period of data and applying correction terms generated from a multiple reference station network has shown that high-quality positioning results can be reliably determined (Rizos *et al.*, 2000). Their results showed centimetre-level accuracy in the horizontal components and 3–5 cm in the up component, even for baseline lengths up to a hundred kilometres. Therefore, the multiple reference station network method can be applied to generate correction terms that reduce the effects of distance-dependent biases such as the residual ionospheric delay and enable high-accuracy positioning with single-frequency L1 GPS receivers.

Instrumentation and general characteristics

Of the 10 CORS located in the study area of the southern LV in eastern Taiwan (Fig. 2), three stations (S105, S104, TTSH) are maintained by the Institute of Earth Sciences Academia Sinica (IESAS), five stations (ERPS, LONT, SINL, TTUN, PEIN) by the Central Weather Bureau and two (TMAM, FUGN) by the Ministry of the Interior. The 10 CORS have been operating since 2008. The existing CORS were apparently not dense enough to account for the near-fault movement detection in the study area consisting of a complicated three-fault system. As mentioned above, the L1 GPS receivers can densify the network for monitoring purposes while seemingly meeting the required positioning accuracy. One major advantage of single-frequency GPS is that the cost of hardware is much



2 Location of single-frequency GPS stations and dual-frequency GPS stations (CORS) in the southernmost Longitudinal Valley of southeastern Taiwan

lower than for dual-frequency equipment (about an order less).

In 2008, we thus installed three L1 stations (RSES, LCBP, FYBP) on the western side of the Coastal Range (Fig. 2), four stations (CLJS, LYJS, BLES, YWES) on the Peinan massif (a package of late Quaternary uplift terrestrial deposits within the LV), six stations (RFES, CLES, DCES, TIPN, DNES, MHES) on the eastern side of the Central Range and four stations (FNES, TGSH, FNLI, FNYN) on the Taitung alluvial plain to better complement the CORS network and to better characterise the surface deformation across the major active faults in the study area.

Networks of L1 GPS receivers mixed with dual-frequency receivers have been previously proposed and tested in active fault zones and for volcano monitoring systems with encouraging results (Chen, 2001; Roberts, 2002; Rizos, 2002). In this study, from the instrument point of view, we have combined a L1 receiver/antenna and an internet transmission device (which sends the data in real-time) to build a near real-time monitoring system (Fig. 3).

In the instrumental aspect, there are three components of our L1 GPS system:

- (i) receiver-antenna all-in-one unit (cone design for navigation; WU810, Allis Communications Company)
- (ii) transmission data device (MOXA)
- (iii) internet devices (ADSL, real-time transmission).

All units of the L1 system were installed on the roof-tops of selected buildings in public schools, which provided free internet transmission in collaboration with the Ministry of Education. The data were sent to the server at the GPS Center of Academia Sinica in Taipei, with a sampling rate of 30 s for 24 h a day, 365 days a year.



3 Entire unit of low-cost single-frequency receiver and transmission devices

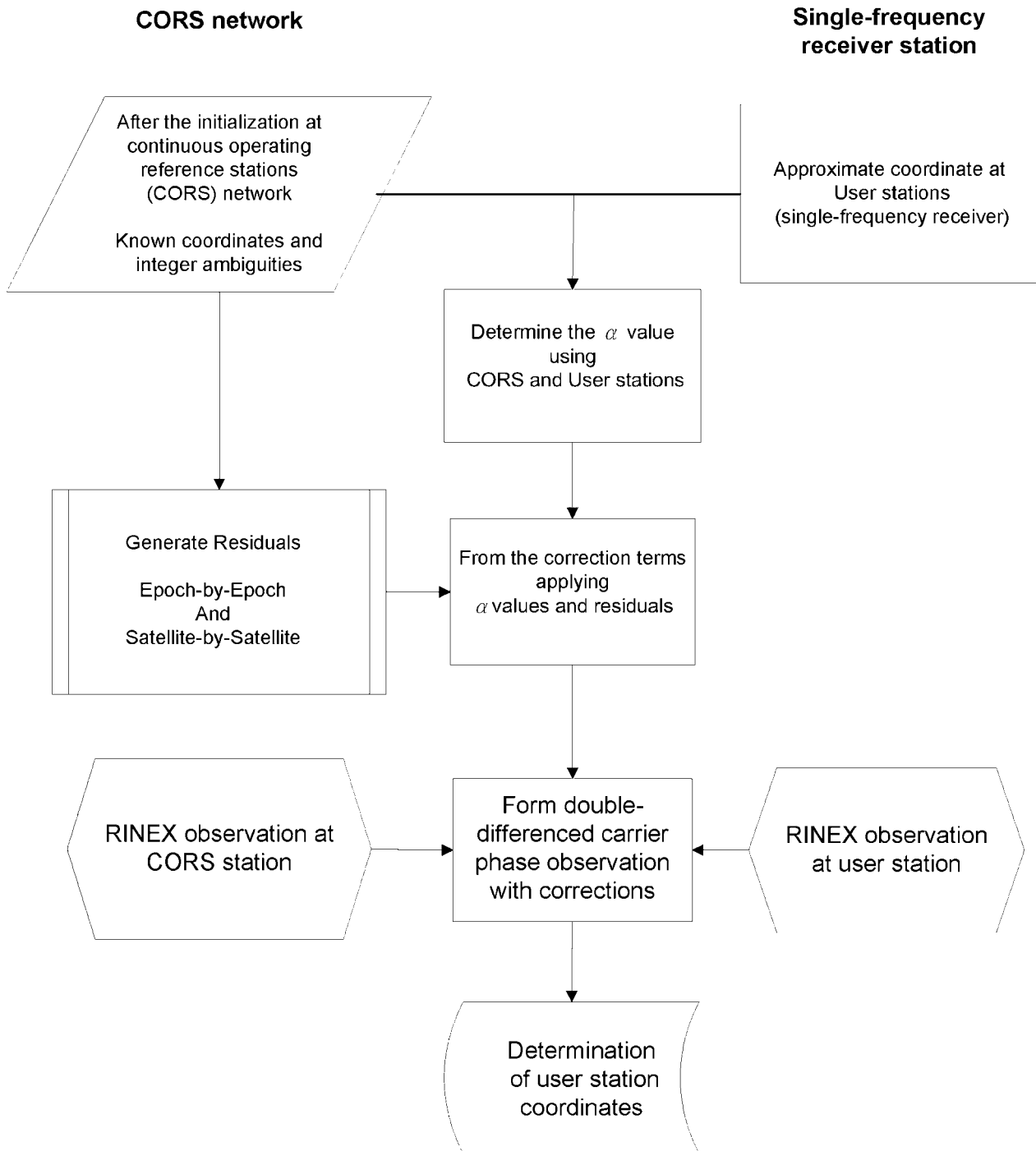
The total cost of one entire unit of such monitoring equipment is less than USD300.

The accuracy of L1 GPS is mainly hampered by the ionospheric delay, which is a distance dependent error (similar to the orbit error and tropospheric delay). To improve the positioning accuracy, a few strategies can be utilised such as reducing the relative distance, applying a local ionospheric model, and adopting the corrections from dual-frequency CORS to mitigate the effect (Wanninger, 1995; Wubbena *et al.*, 1996; Han and Rizos, 1996; Chen, 2001). In this study, we deal with a relatively short distance of under 30 km for the GPS network. We intend to test our data quality and its characteristics in terms of positioning accuracy and precision by applying two methods: (i) local ionospheric model and (ii) correction terms from dual-frequency CORS.

Methodology of data processing

In the processing procedure, we adopt the International GNSS Service final orbit. We also use multipath error reduction techniques, so that the effect of orbit and multipath errors can be assumed to be significantly mitigated. Hence, the main biases in L1 positioning are the ionospheric and tropospheric delays. For the L1 carrier-phase ambiguity resolution algorithm, the standard atmospheric model can be applied to determine the residual tropospheric zenith delay, followed by estimates every 2–4 h per station simultaneously with the station coordinates using a least squares adjustment (Hopfield, 1969; Saastamoinen, 1973; Niell, 1996; Hofmann-Wellenhof *et al.*, 1997). For long-period datasets (several hours) the success rate of ambiguity resolution and the accuracy of positioning estimation depend on the disturbance of the ionosphere, since the ionospheric delay cannot be totally mitigated using procedures for dual-frequency receivers (Rothacher and Mervart, 1996).

The ionospheric delay is one of the signal propagation biases that affect both pseudo-range and carrier-phase measurements. However, the special characteristics of the integrated carrier phase observable lead to an additional type of constant bias known as the phase ambiguity (Rizos, 1999). There are a number of factors influencing the magnitude of the ionospheric delay, including the latitude of the receiver, seasonal variation, time of day, signal observation being made and the level of



4 Procedure for generating correction terms from the CORS network and processing method for its application for single-frequency GPS receiver

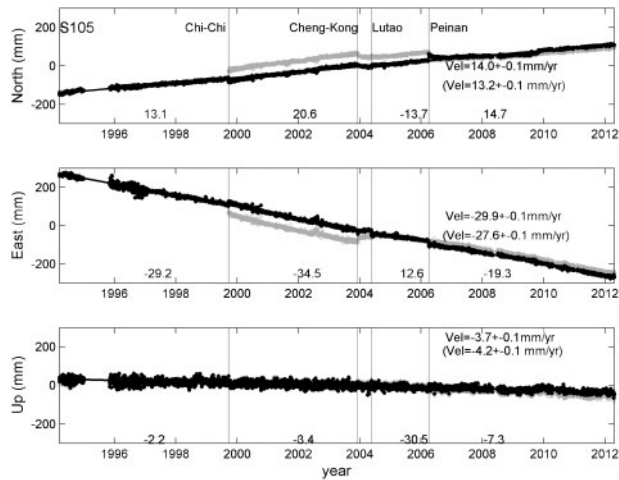
solar activity at the time of observation (Klobuchar, 1991). However, for the low-cost L1 receiver, a few strategies can be utilised to mitigate the effect of the ionospheric delay such as reducing the relative distance, applying a local ionospheric model and acquiring corrections from a reference network of dual-frequency GPS stations. Hereafter we describe how we used these two latter most common methods to improve the accuracy of our single-frequency GPS stations in the study area.

Local ionospheric model

In general, epoch-by-epoch, satellite-by-satellite ionospheric delay can be estimated by using the double-differenced observation equation for the geometry-free

linear combination of the carrier-phase measurements referring to a set of two receivers and two satellites (Han, 1997). We employ the Bernese Version 5.0 software, which applies a single-layer model based on the corresponding mapping function (Dach *et al.*, 2007) to estimate the local ionospheric model. The resulting model is very useful and can be applied to further analysis for single-frequency GPS users (Schaer *et al.*, 1995).

For processing, we estimate the local ionospheric delay model from the ten CORS in the study area (Fig. 2), after fixing the ambiguities and coordinates of the CORS. We thus obtain the single-layer ionospheric model. We then apply this local ionospheric model to test the positioning accuracy of the L1 stations.



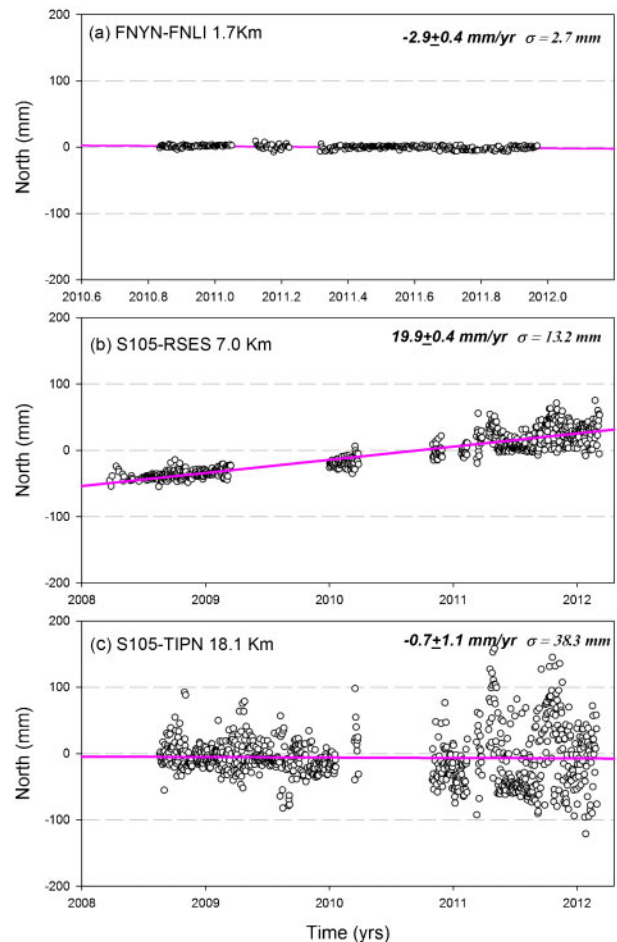
5 Time series of daily solutions for CORS station S105 in 1995–2012, after removing the co- and post-seismic effects of the regional and local large earthquakes. The gray dots correspond to original data before calibration. Vel: interseismic velocity of S105 in ITRF2005 frame (Vel in parenthesis indicates velocity before removing co- and post-seismic effects)

Correction terms from nearby CORS

During the past two decades, several studies have applied corrections from a reference station network to mitigate the distance-dependent error and to improve positioning accuracy in real-time GPS kinematic studies with satisfactory results (Hofmann-Wellenhof *et al.*, 1997; Wubbena *et al.*, 1996; Wanninger, 1997; Raquet *et al.*, 1998; Janssen and Rizos, 2003). Other studies used virtual reference stations to enhance the positioning accuracy for different applications (Marel, 1998; Chen *et al.*, 2001; Landau *et al.*, 2002; Landau *et al.*, 2007).

These kinds of corrections are essentially based on an epoch-by-epoch, satellite-by-satellite approach based on CORS. If the behaviour of the atmospheric delay can be modelled for the area covered by the CORS, the atmospheric delay could be estimated and mitigated on an epoch-by-epoch and satellite-by-satellite basis to help improve the positioning accuracy of the single-frequency stations in the same area (Wu, 1994; Han, 1997). The basic operational algorithm for generating corrections demands two requirements to support high-accuracy positioning. First the ambiguities, coordinates and other parameters need to be estimated correctly using the CORS, followed by fixing the estimated ambiguities and coordinates to generate the distance-dependent errors for different GPS signals. Secondly, the correction generation should follow corresponding algorithms such as the weighted differential GPS method (Klobuchar, 1987; Qiu *et al.*, 1995; Gao and Liu, 2002; Zhang and Feng, 2005). In this paper, we follow the weighted differential GPS method proposed by Wu (1994) to generate the corrections.

The flowchart for generating the correction terms and the processing procedure for single-frequency L1 GPS receivers is illustrated in Fig. 4. There are two main parts of the procedure: the upper part combines CORS and continuous L1 GPS receivers to generate the correction terms, and the lower part forms double-differenced observations with correction terms to estimate the ambiguities and the baseline between the



6 Times series showing daily solutions of relative positions a 1.7 km baseline FNYN-FNLI, b 7.0 km baseline S105-RSES and c 18.1 km baseline S105-TIPN. Linear trends are approximated with least-square technique. The standard deviations (σ) of the fitted lines are determined after de-trending

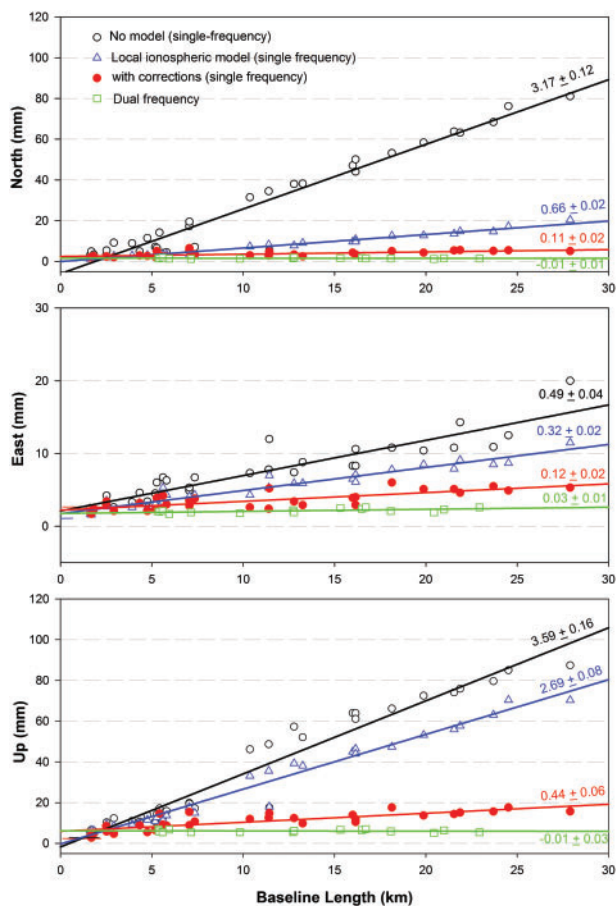
CORS and L1 receiver. In practice, the coordinates and ambiguities of the CORS need to be known in order to fix these parameters to output the residual (the residual is mainly constituted of the atmospheric delay bias). Depending on the location of the L1 receiver within the CORS network, we can then determine the weight of the residual (i.e. the correction term) for the baseline between one of the CORS and the L1 station. Once the correction term is determined, the ambiguities and the baseline components can be estimated.

Estimation of positioning accuracy in southernmost LV

Positioning accuracy

Daily solutions using the three algorithms described above, i.e. (A) without any corrections, (B) applying the local ionospheric model and (C) with correction terms from dual-frequency stations, were computed for the 17 L1 (single-frequency) GPS stations and compared to solutions from dual-frequency stations in the study area.

In practice, we used CORS station S105 as the reference (Fig. 5) to calculate the relative positions of daily solutions for each L1 station. The time series of station positions relative to S105 can thus be determined



7 Standard deviations using four different algorithms applied on estimation of GPS station positions with respect to baseline length in southernmost LV, Taitung, Taiwan

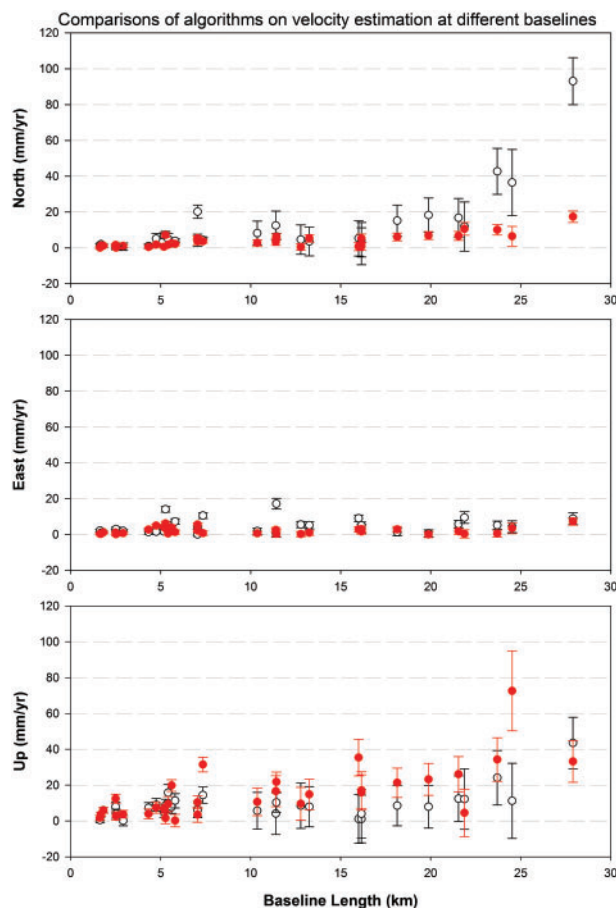
without any corrections. We then estimated the relative velocity as the linear trend of the time series and also obtained its standard deviation. Figure 6 shows three examples with different baselines of 1.7, 7.0 and 18.1 km length for three L1 stations, FNLI, RSES and TIPN, respectively. The scatters of positioning, which are quantitatively exhibited by standard deviations after de-trending the linear approximation, are larger as the baseline length increases (Fig. 6).

Figure 7 illustrates the standard deviations of daily station positioning for each relative distance (i.e. baseline length) for a time span of 3–4 years (2008–2012) after removing the linear trend. These represent solutions using the aforementioned three different approaches (Methods A, B and C) compared to those obtained with dual-frequency stations. Detailed results are shown in Table 1. Overall, the standard deviations of the L1 positioning show a linear relationship with baseline length. For

Table 1 Accuracy (standard deviation versus baseline) from different estimation algorithms*

Method	North/mm km ⁻¹	East/mm km ⁻¹	Up/mm km ⁻¹
A	3.17 ± 0.12,	0.49 ± 0.04	3.59 ± 0.16
B	0.66 ± 0.02	0.32 ± 0.02	2.69 ± 0.08
C	0.11 ± 0.02	0.12 ± 0.02	0.44 ± 0.06
Reference	0.01 ± 0.01	0.03 ± 0.01	0.01 ± 0.03

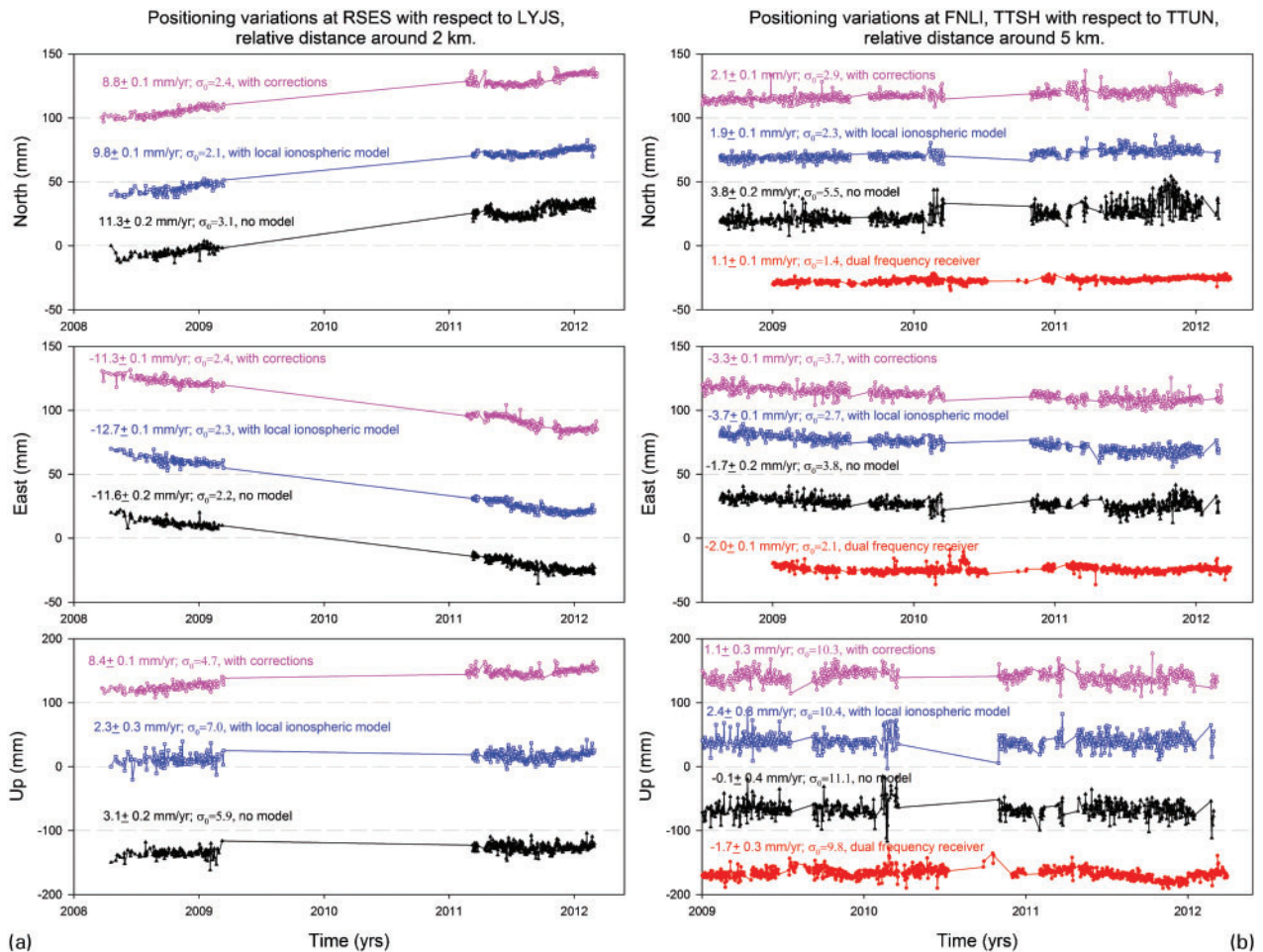
*Method A: no model; B: local ionospheric model; C: applying corrections; Reference: dual-frequency.



8 Comparisons of the algorithms A and B with Method C (favoured calibration algorithm) for velocity estimation. Solid circle denotes the difference of velocity estimation between applying no model (Method A) and applying the correction algorithm (Method C). The open circle represents the velocity difference between applying the local ionospheric model (Method B) and applying the correction algorithm (Method C)

instance, the slopes of standard deviation/baseline are 3.17 ± 0.12 , 0.49 ± 0.04 and 3.59 ± 0.16 mm km⁻¹, respectively in the north, east and up components without any calibration (Method A). The slopes of standard deviation versus baseline length decrease significantly when applying the two calibration methods: 0.66 ± 0.02 , 0.32 ± 0.02 , and 2.69 ± 0.06 mm km⁻¹ respectively for utilising the local ionospheric model (Method B), and 0.11 ± 0.02 , 0.12 ± 0.02 , 0.44 ± 0.06 mm km⁻¹ respectively with correction terms (Method C). This implies that positioning accuracy can reach 3 mm in the horizontal components and 13 mm in the vertical component, after applying the correction term algorithm (Method C) for relative distances less than 30 km.

For this testing range, as expected the dual-frequency solutions (Method Reference) do not have any significant baseline effect on accuracy. Compared with different algorithms applied to L1 solutions, the order of accuracy by methods is C, B and A respectively. For instance, for the 27 km relative distance, there are less than 3, 3 and 13 mm differences in the north, east and up component between the solutions from the dual-frequency receiver and the L1 observations with correction algorithm applied (Method C). There are 18, 9 and 72 mm



9 Station scatter, velocity estimations and their standard deviations for a 2 km baseline RSES to LYJS and b 5 km baseline FNL1 to TTUN. Note that the lowest results (red dots) of each component subplot are derived from nearby dual-frequency stations (TTSH to TTUN)

differences in the north, east and up component when applying the local ionospheric model algorithm (Method B), and there are more than 85, 13 and 95 mm differences in the north, east and up component when no correction algorithm is applied (Method A).

Comparing Method B and Method C, the north component can be significantly improved for both methods, but there is no obvious refinement in the up component for Method B. This implies that the ionospheric delay can be mitigated but the tropospheric delay is still affecting the positioning accuracy. Focusing on the correction algorithm approach of Method C, the accuracies denote both horizontal and vertical components have been significantly improved and close to mm level compared to the dual-frequency observations, even at a relative distance of 30 km.

Accuracy of velocity estimates

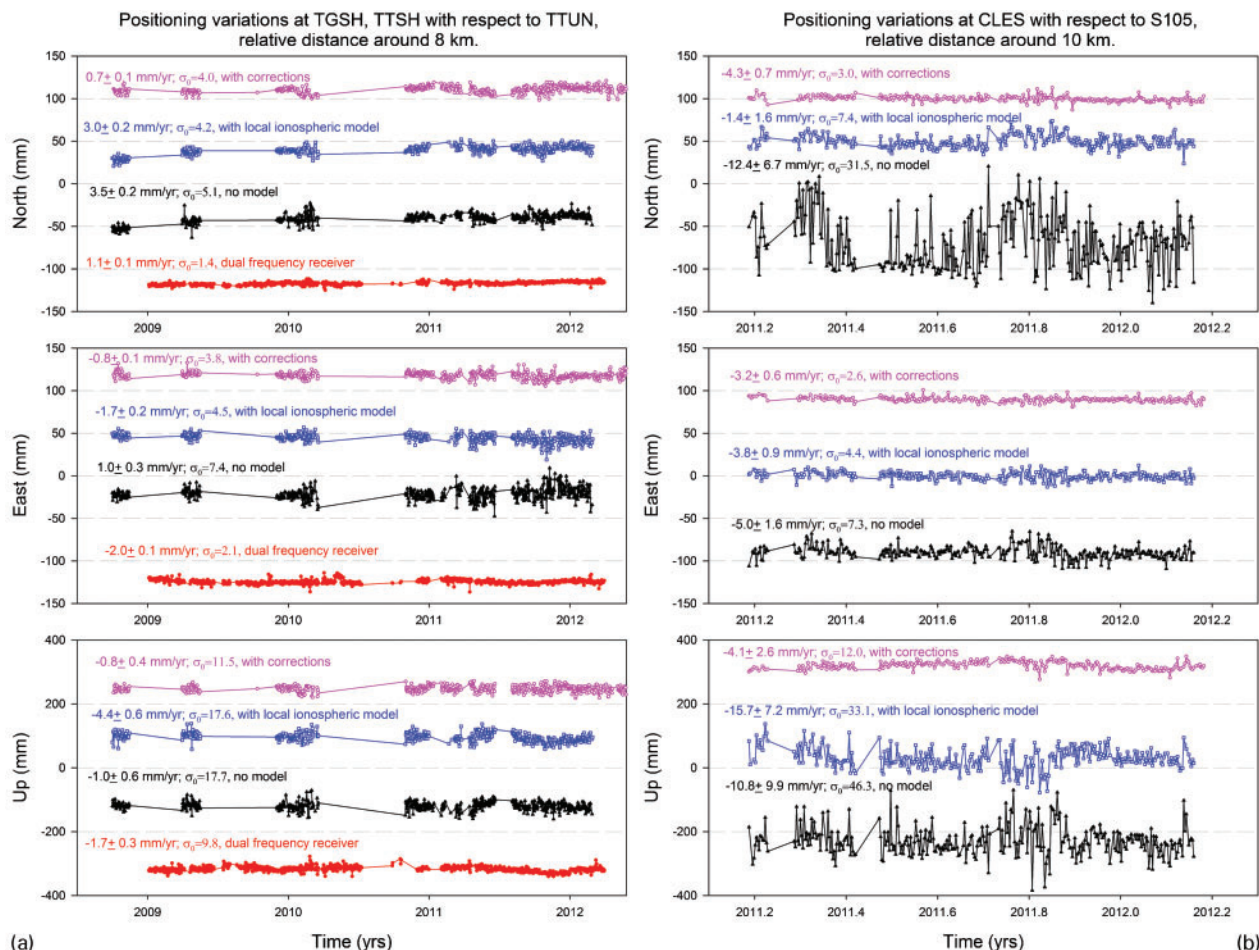
As the GPS station velocity is often used as a quantity to characterise surface deformation, we also compared the estimates of station velocity from the L1 stations by the above three methods. Again, we selected the CORS S105 as the main reference station to calculate the relative distance for L1 stations, so the time series can be estimated for the above three methods. We then applied the station velocity of S105 (Fig. 5), estimated from the CORS network, to calculate the station velocity for each L1 station. Assuming the station velocity is a linear

variation, the inter-seismic station velocity can be obtained as

$$y(t_i) = a + bt_i \quad (1)$$

where a and b represent the intercept and the linear variation of the inter-seismic velocity, respectively.

The velocity estimation of each L1 station in the study area was calculated using the three correction algorithms (Methods A, B and C). Figure 8 shows the discrepancy of station velocity with respect to the baseline length of stations in the study area by using the aforementioned three algorithms (methods). Because Method C has proven to be satisfactory for the positioning accuracy in the study area, as described above, we used the station velocity determined by Method C as the reference in order to compare it to the results of Methods A and B. As expected, there are no obvious differences for the three algorithms when the relative distance is less than 5 km. The differences reach more than 10 mm/year for baseline lengths greater than 10 km in the horizontal and vertical components. Most of the differences show less than 20 mm/year in the comparison between applying no model and correction algorithm. Comparing the local ionospheric model with the correction algorithm, the difference is less than 6 mm/year in the horizontal components for baselines less than 20 km, but in the vertical component the difference reaches 20 mm/year for a baseline length of 15 km. Hence, there is not only an



10 Station scatter, velocity estimations, and their standard deviations for a 8 km baseline TGSH to TTUN and b 10 km baseline CLES to S105. Note that the lowest result (red dots) of each component subplot is derived from nearby dual-frequency stations (TTSH to TTUN)

improvement in the horizontal velocity but also in the vertical velocity when applying the correction algorithm.

In summary, analysing the comparison of three algorithms for velocity estimation, a significant difference occurs for baselines larger than 5 km between the no model case and the correction algorithm. There is no obvious discrepancy of station velocity in the east component with the local ionospheric model and with the correction algorithm, and as the relative distance increases the difference increases. It appears that the ionospheric delay affects the positioning accuracy more in the north component than in the east component. Meanwhile, the difference increases in the vertical component with increasing relative distance due to the tropospheric delay error still affecting the positioning.

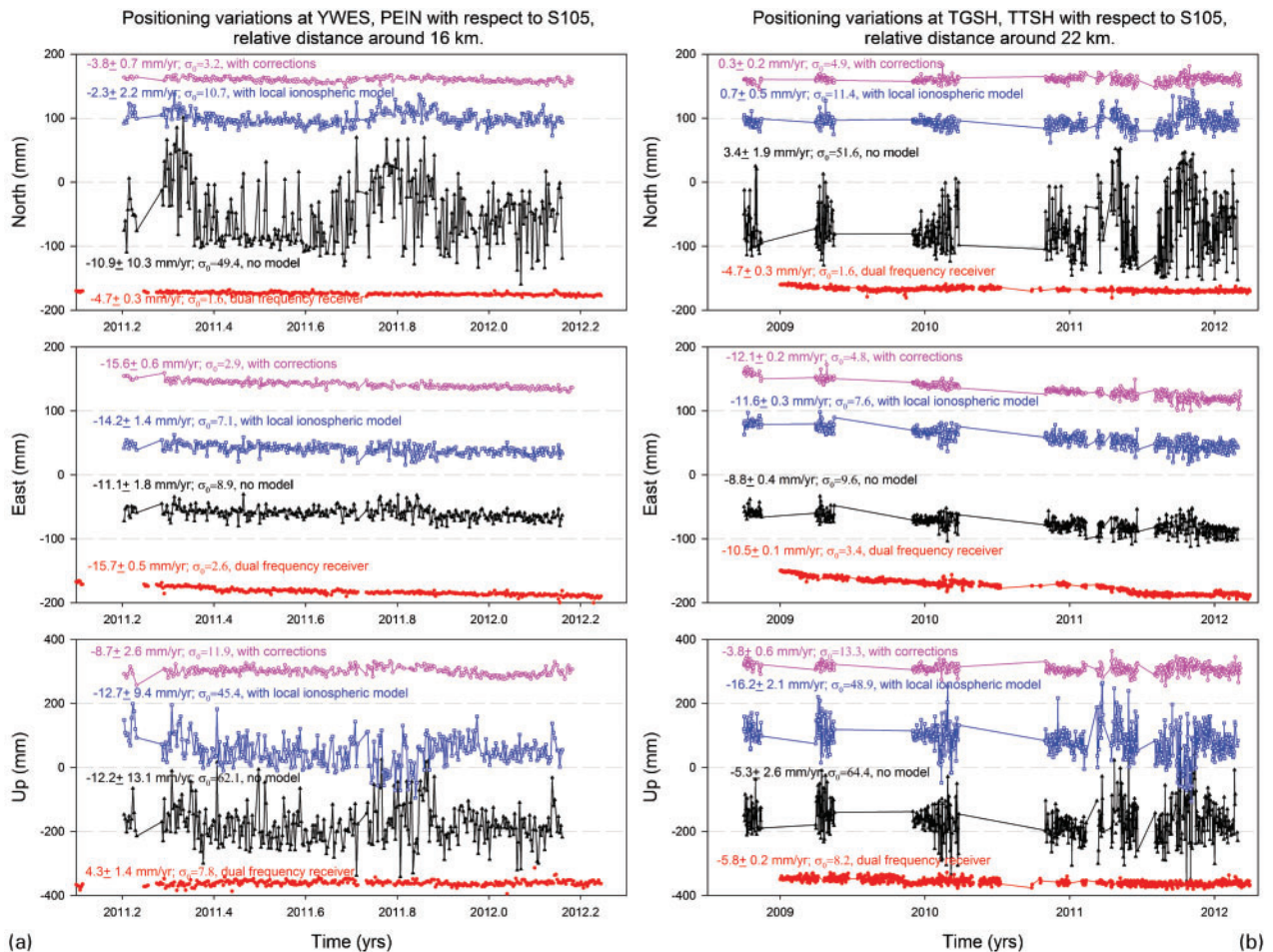
Example tests on baseline accuracy

In this section, we show the results of some examples of L1 stations in the study area after applying the three algorithms and discuss how they affect positioning accuracy as a function of baseline length. We illustrate the position scatter by plotting station position estimates through time for different baseline lengths: 2 and 5 km (Fig. 9a and b), 8 and 10 km (Fig. 10a and b), and 16 and 22 km (Fig. 11a and b). We added data from a nearby dual-frequency CORS (represented in red in each plot) for comparison.

For the short 2 km baseline, we selected a pair of L1 stations, LYJS to RSES (see location in Fig. 2), because

there is no L1 station near S105. The results of relative station velocity (Fig. 9a) show in the north component: (a) 8.8 ± 0.1 mm/year ($\sigma=2.4$ mm) with corrections applied, (b) 9.8 ± 0.1 mm/year ($\sigma=2.1$ mm) with a local ionospheric model and (c) 11.3 ± 0.2 mm/year ($\sigma=3.1$ mm) with no model algorithms. For the east component, we obtain -11.3 ± 0.1 mm/year ($\sigma=2.4$ mm), -12.7 ± 0.1 mm/year ($\sigma=2.3$ mm) and -11.6 ± 0.2 mm/year ($\sigma=2.2$ mm) for the three approaches respectively. Finally, in the vertical component, the results show 8.4 ± 0.1 mm/year ($\sigma=4.7$ mm), 2.3 ± 0.3 mm/year ($\sigma=7.0$ mm) and 3.1 ± 0.2 mm/year ($\sigma=5.9$ mm) for the three algorithms, respectively. There are practically no obvious differences in both the horizontal and vertical components in terms of station velocity and standard deviation for the 2 km baseline when comparing the three algorithms. Although a nearby CORS station does not exist for comparison at this distance range, the position scatters, which can be indicated by standard deviations, are within a reasonable range with relatively small values for the horizontal components, but larger values for the up component.

In the 5 km baseline case (Fig. 9b), TTUN (CORS) to FNLI (L1), the results show relative station velocities of 2.1 ± 0.1 mm/year ($\sigma=2.9$ mm), 1.9 ± 0.1 mm/year ($\sigma=2.3$ mm) and 3.8 ± 0.2 mm/year ($\sigma=5.5$ mm) in the north component obtained with corrections, local ionospheric model and no model algorithms, respectively. In



11 Station scatter, velocity estimations, and their standard deviations for *a* 16 km baseline YWES to S105 and *b* 22 km baseline TGSH to S105. Note that the lowest result (red dots) of each component subplot is derived from nearby dual-frequency stations (PEIN to S105 and TTSH to S105)

the east component, we obtained -3.3 ± 0.1 mm/year ($\sigma=3.7$ mm), -3.7 ± 0.1 mm/year ($\sigma=2.7$ mm) and -1.7 ± 0.2 mm/year ($\sigma=3.8$ mm), respectively. For the up component, results reveal 1.1 ± 0.3 mm/year ($\sigma=10.3$ mm), 2.4 ± 0.6 mm/year ($\sigma=10.4$ mm) and -0.1 ± 0.4 mm/year ($\sigma=11.1$ mm). In this subplot of Fig. 9b, a nearby pair of dual-frequency CORS (TTUN to TTSH) has been used to compare with single-frequency data and is presented in the lowest graph. The standard deviation of the no model algorithm shows a larger scatter and a larger discrepancy compared to the other algorithms, presumably due to the ionospheric delay affecting the observation. By comparing the velocity estimation of dual-frequency with single-frequency and applying the correction algorithm, there are 1–2 mm/year differences of velocity in the horizontal components and 3 mm/year in the up component.

For the 8 km baseline, TTUN (CORS) to TGSH (L1) (Fig. 10a), the algorithm with corrections shows smaller standard deviations than the other two algorithms and the velocity estimation results are close to the dual-frequency observation. Under the effect of ionospheric delay, the results with the local ionospheric model algorithm are better than that without model algorithm in the horizontal component, but no improvement is evident in the up component.

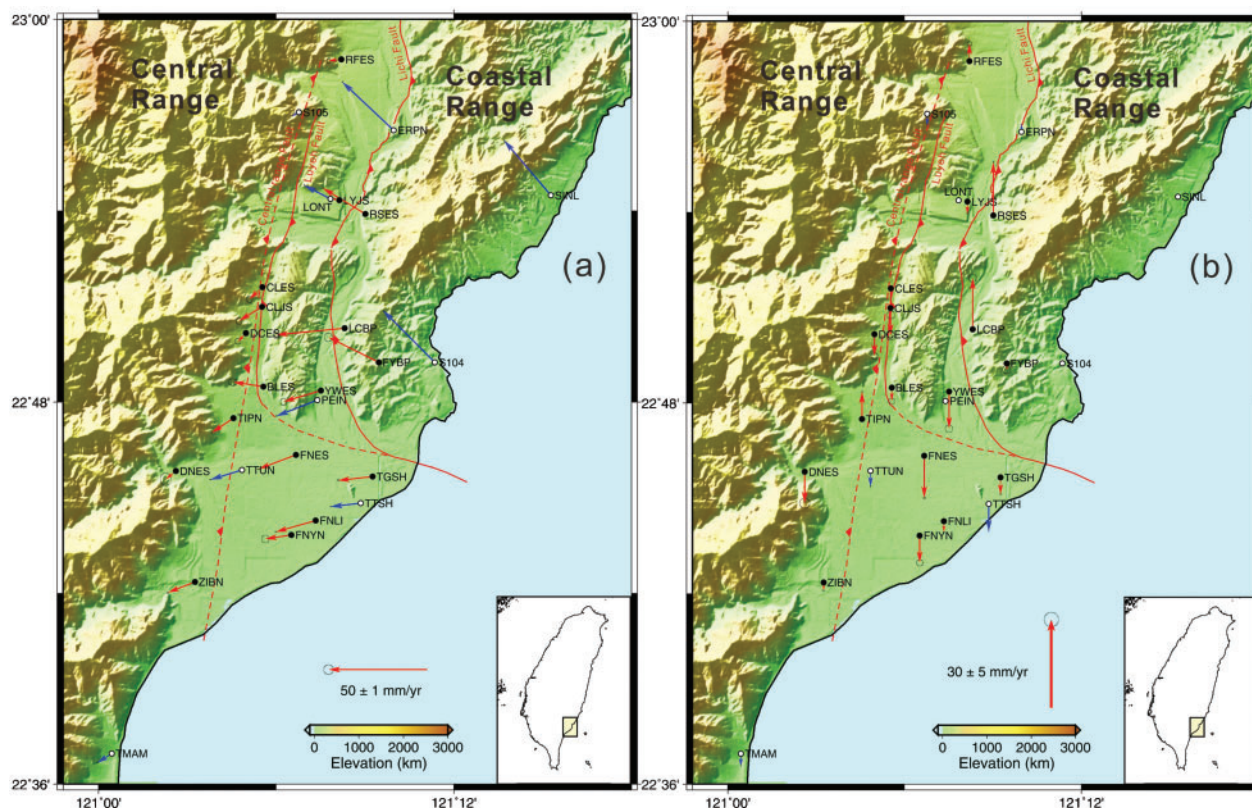
For longer baselines of 10, 16 and 22 km (Figs. 10b, 11a and b), the algorithm with corrections presents a big

improvement in decreasing the standard deviation of position scattering, much more than the other two algorithms. The accuracy of velocity estimation and the positioning results compared to the dual-frequency stations (when applicable in the same local area) indicate a general good agreement with those obtained from the correction algorithm. As expected, the results with the local ionospheric model algorithm are much better than that without model algorithm in the horizontal component for longer baselines due to turbulences in the ionosphere. Also the standard deviation shows a significant improvement with the use of the local ionospheric model algorithm for distances larger than 10 km, but this only slightly affects the results obtained from the correction algorithm.

In summary, our test examples for different baseline lengths within the range of the study area (i.e. 2 to 22 km) have shown that the determined station velocity of an L1 receiver with correction term applied is general in good agreement with the traditional dual-frequency GPS receiver, in particular in the horizontal components.

Optimal velocity field in Taitung area

The station velocities derived from the low-cost single-frequency stations densifying the CORS network in the Taitung area are shown in Fig. 12. The station velocity fields combining dual- and single-frequency GPS stations



12 *a* horizontal velocity field and *b* vertical velocity field in Taitung area, Taiwan. Blue vectors represent CORS and red vectors denote L1 GPS results

in the Taitung area are illustrated in the ITRF2005 reference frame. As shown in the figure, the coverage of the combined GPS network is able to characterise the three-fault system in the Taitung area. The horizontal velocity field (Fig. 12*a*) shows left-lateral behaviour of the Lichi Fault. The surface deformation was concentrated across the Longitudinal Valley Fault, on both surface strands: the Luyeh Fault to the west and the Lichi Fault to the east. The eastern side of the Central Range exhibited an intriguing southwest-moving pattern, which might be interpreted as a mountain-parallel flow or lateral extrusion. The vertical velocity field (Fig. 12*b*) denotes rapid uplift (about 25–30 mm/year) on the western side of the Coastal Range in the immediate hanging wall of the Lichi Fault. By contrast, the Taitung alluvial region and the eastern margin of the Central Range represent a subsidence movement pattern.

Concluding remarks

In this study, 17 low-cost single-frequency GPS receivers have been deployed to intensify and complement ten CORS in the Taitung area, southeastern Taiwan since 2008. Three position estimation algorithms for correcting daily solutions of low-cost, single-frequency L1 receivers over a range of relative distances (less than 30 km), including no correction, local ionospheric model and correction terms from a local dual-frequency CORS network, have been analysed to investigate their validity and uncertainty of the station velocities for the period 2008–2012. Some conclusions can be drawn as follows.

1. When the relative distance is longer than 5 km, the ionospheric delay should be considered the main error source in L1 positioning in southeastern Taiwan.

2. The local ionospheric model can improve the accuracy in the horizontal component, but provides little in regards to improving the vertical component.

3. For short baselines of less than 3 km, there are no obvious differences in the horizontal component when comparing the three algorithms.

4. The standard deviations of the linear trends based on daily solutions for the L1 stations show a significant increase after the relative distance is greater than 10 km when using only the local ionospheric model algorithm, but remain small when using the correction algorithm.

5. The correction algorithm can significantly improve the positioning accuracy of low-cost single-frequency L1 receivers to the millimetre level (3 mm in the horizontal components and 13 mm in the vertical component), even when the relative distance reaches 30 km in southeastern Taiwan.

6. Detailed GPS velocity fields, horizontal and vertical, can be obtained in the Taitung area to clarify near-fault movement behaviour from a combined network of dense continuously operating dual- and single-frequency GPS stations.

Acknowledgements

The authors would like to express their sincere thanks to their colleagues and assistants who have devoted efforts to the field installation of L1 GPS stations for this study. The International GNSS Service has provided the precise ephemerides for data processing. We also thank two anonymous reviewers for their constructive comments and suggestions, which helped to improve the manuscript. This research was supported by the Taiwan Earthquake Research Center (TEC) funded through the

National Science Council with the grants NSC101-2116-M-001-010 and NSC102-2116-M-001-016. The paper is a contribution of the Institute of Earth Sciences, Academia Sinica, IESAS1852, and the TEC (contribution number: 00098).

References

- Blewitt, G., 1989. Carrier phase ambiguity resolution for the Global Positioning System applied to geodetic baselines up to 2000 km. *Journal of Geophysical Research*, 94(B8), pp. 10187–3.
- Biq, C. C., 1965. The eastern Taiwan rift. *Petrol. Geol. Taiwan*, 4, pp. 93–106.
- Chen, H. Y., Rizos, C. and Han, S., 2001. From simulation to implementation: low-cost densification of permanent GPS networks in support of geodetic applications. *Journal of Geodesy*, 75(9/10), pp. 515–26.
- Chen, H. Y., 2001. *A study on real-time medium-range carrier-phase-based GPS multiple reference stations*. PhD dissertation, UNISURV rept. no. S-64. School of Surveying and Spatial Information Systems, The University of New South Wales, Australia.
- Chen, H. Y., Lee, J. C., Tung, H., Yu, S. B., Hsu, Y. J. and Lee, H., 2012. Determination of vertical velocity field of southernmost Longitudinal Valley in eastern Taiwan: a joint analysis of leveling and GPS measurements. *Terrestrial, Atmospheric and Oceanic Sciences*, 23(4), pp. 355–76.
- Chen, H. Y., Lee, J. C., Tung, H., Yu, S. B., Hsu, Y. J. and Lee, H., 2013. A new velocity field from a dense GPS array in southeastern Taiwan. *Terrestrial, Atmospheric and Oceanic Sciences*, 24(5), pp. 837–62.
- Dach, R., Hugentobler, U., Fridez, P. and Meindl, M., 2007. Bernese GPS software Version 5.0. Astronomical Institute, University of Bern.
- Gao, Y. and Liu, Z. Z., 2002. Precise Ionosphere Modeling Using Regional GPS Network Data. *Journal of Global Positioning Systems*, 1(1), pp. 18–24
- Han, S., 1997. *Carrier phase-based long-range gps kinematic positioning*. PhD dissertation, UNISURV rept. no. S-49. School of Geomatic Engineering, The University of New South Wales.
- Han, S. and Rizos, C., 1996. GPS network design and error mitigation for real-time continuous array monitoring systems. *Proceedings of the International Technical Meeting of The Institute of Navigation, GPS ION*, 96. Kansas City, MO, USA, 17–20 September 1996. pp. 1827–36.
- Hofmann-Wellenhof, B., Lichtenegger, H. and Collins, J., 1997. *GPS: Theory and practice*. 4th, revised ed. New York: Springer Wien.
- Hopfield, H., 1969. Two-Quartic Tropospheric Refractivity Profile for Correcting Satellite Data. *Journal of Geophysical Research*, 74(18), pp. 4487–99.
- Janssen, V. and Rizos, C., 2003. A mixed-mode GPS network processing approach for deformation monitoring applications. *Survey Review*, 37(287), pp. 2–19.
- Klobuchar, J. A., 1987. Ionospheric time-delay algorithm for single-frequency GPS users. *IEEE Transactions on Aerospace and Electronic Systems*, 23(3), pp. 325–31.
- Klobuchar, J. A., 1991. Ionospheric effects on GPS. *GPS world*, 2(4), pp. 48–51.
- Landau, H., Vollath, U. and Chen, X., 2002. Virtual reference station systems. *Journal of Global Positioning Systems*, 1(2), pp. 137–43.
- Landau, H., Chen, X., Kipka, A. and Vollath, U., 2007. Network RTK: Getting ready for GNSS modernization. *GPS World*, 18(4), pp. 50–5.
- Lee, J. C., Angelier, J., Chu, H. T., Yu, S. B. and Hu, J. C., 1998. Plate-boundary strain partitioning along the sinistral collision suture of the Philippine and Eurasian plates: Analysis of geodetic data and geological observation in southeastern Taiwan. *Tectonics*, 17(6), pp. 859–71.
- Lu, C. Y. and Hsu, K. J., 1992. Tectonic evolution of the Taiwan mountain belt. *Petrol. Geol. Taiwan*, 27, pp. 21–46.
- Marel, H. van der, 1998. Virtual GPS Reference Stations in the Netherlands, *Proceedings of the International Technical Meeting of The Institute of Navigation, GPS ION*, 98. Nashville, TN, USA, 15–18 September 1998. pp. 49–58.
- Niell, A. E., 1996. Global Mapping Functions for the Atmosphere Delay at Radio Wavelengths. *Journal of Geophysical Research*, 101(B2), pp. 3227–46.
- Qiu, W., Lachapelle, G. and Cannon, M. E., 1995. Ionospheric effect modelling for single frequency GPS users. *Manuscripta Geodaetica*, 20(2), pp. 96–109.
- Raquet, J. F., Lachapelle, G. and Melgrad, T., 1998. Test of a 400 km x 600 km network of reference receivers for precise kinematic carrier-phase positioning. *Proceedings of the International Technical Meeting of The Institute of Navigation, GPS ION*, 98. Nashville, TN, USA, 15–18 September 1998. pp. 407–16.
- Rizos, C., 1999. Precise satellite positioning: challenges & prospects. Presented at *GPS/GIS Showcase*. Nanyang Technological University, Singapore, 19–20 November 1999.
- Rizos, C., Han, S. and Chen, H. Y., 2000. Regional-scale multiple reference stations for real-time carrier phase-based GPS positioning: a correction generation algorithm. *Earth, Planets & Space*, 52(10), pp. 795–800.
- Rizos, C., 2002. Network RTK research and implementation - a geodetic perspective. *Journal of Global Positioning Systems*, 1(2), pp. 144–50.
- Roberts, C., 2002. *A continuous low-cost GPS-based volcano deformation monitoring system in Indonesia*. PhD thesis, School of Surveying & Geospatial Engineering. University of New South Wales, Sydney, Australia.
- Rothacher, M. and Mervart, L., 1996. Bernese GPS Software, Version 4.0. Astronomical Institute, University of Berne.
- Saastamoinen, J., 1973. Contributions to the theory of atmospheric refraction. *Journal of Geodesy*, 107(1), pp. 13–34.
- Schaer, S., Beutler, G., Mervart, L., Rothacher, M. and Wild, U., 1995. Global and regional ionosphere models using the GPS double difference phase observable, in *IGS Workshop Proceedings on Special Topics and New Directions*, GFZ, Potsdam, Germany, 15–17 May 1995. pp. 77–92.
- Shyu, J. B. H., Sieh, K., Chen, Y. G., Chuang, R. Y., Wang, Y. and Chung, L. H., 2008. Geomorphology of the southernmost Longitudinal Valley fault: Implications for evolution of the active suture of eastern Taiwan. *Tectonics*, 27, TC1019, doi:10.1029/2006TC002060.
- Wanninger, L., 1995. Improved ambiguity resolution by regional differential modelling of the ionosphere, *Proceedings of the International Technical Meeting of The Institute of Navigation, GPS ION*, 95. Palm Springs, CA, USA, 12–15 September 1995. pp. 55–62.
- Wanninger, L., 1997. Real-time differential GPS-error modelling in regional reference station networks. *Proceeding of IAG Symposium*, Rio de Janeiro, Brazil, 3–9 September 1997. Berlin: Springer, 118. pp. 86–92.
- Wu, J. T., 1994. Weighted differential GPS method for reducing ephemeris error. *Manuscripta Geodaetica*, 20, pp. 1–7.
- Wu, Y. M., Chen, Y. G., Chang, C. H., Chung, L. H., Teng, T. L., Wu, F. T. and Wu, C. F., 2006. Seismogenic structure framework in a tectonic suture zone: with new constraints from 2006 Mw6.1 Taitung earthquake. *Geophysical Research Letters*, 33(22), Art. No. L22305.
- Wubbena, G., Bage, A., Seeber, G., Boder, V. and Hankemeier, P., 1996. Reducing distance dependent errors for real-time precise DGPS applications by establishing reference station networks. *Proceedings of the International Technical Meeting of The Institute of Navigation, GPS ION*, 96. Kansas City, MO, USA, 17–20 September 1996. pp. 1845–52.
- Yu, S. B., Jackson, D. D., Yu, G. K. and Liu, C. C., 1990. Dislocation model for crustal deformation in the Longitudinal Valley area, eastern Taiwan. *Tectonophysics*, 183, pp. 97–109.
- Yu, S. B. and Kuo, L. C., 2001. Present-day crustal motion along the Longitudinal Valley fault, eastern Taiwan. *Tectonophysics*, 333, pp. 199–217.
- Yu, S. B., Chen, H. Y. and Kuo, L. C., 1997. Velocity field of GPS stations in the Taiwan area. *Tectonophysics*, 274, pp. 41–59.
- Zhang, Y. and Feng, Y., 2005. Interpolating residual zenith tropospheric delays for improved regional area differential GPS positioning. *Navigation*, 52(3), pp. 179–87.